15

Equivalent Circuit Models for Optical Amplifiers

Jau-Ji Jou[1] and Cheng-Kuang Liu[2]
[1]*National Kaohsiung University of Applied Sciences*
[2]*National Taiwan University of Science and Technology*
Taiwan

1. Introduction

Electrical equivalent circuit models for optical components are useful as they allow existing, well-developed circuit simulators to be used in design and analysis of optoelectronic devices. A circuit simulator also allows integration with electrical components (package parasitic, laser driver circuit, etc.). Equivalent circuit models were developed and investigated for some optoelectronic circuit elements, including p-i-n diodes, laser diodes, and waveguide modulators (Bononi et al., 1997; Chen et al., 2000; Desai et al., 1993; Jou et al., 2002; Mortazy & Moravvej-Farshi, 2005; Tsou & Pulfrey, 1997).

The features of erbium-doped fiber amplifiers (EDFAs) are continuously investigated because of their great importance in optical communication systems. In order to design and analyze the characteristics of EDFAs, it is essential to have an accurate model. A dynamic model of EDFAs is helpful to understand the transient behavior in networks. The EDFA dynamics can also be used to monitor information in optical networks (Murakami et al., 1996; Shimizu et al., 1993). In this chapter, using a new circuit model for EDFAs, the static and dynamic characteristics of EDFAs can be analyzed conveniently through the aid of a SPICE simulator. The dc gain, amplified spontaneous emission (ASE) spectrum, frequency response and transient analysis of EDFAs can be simulated.

Semiconductor optical amplifiers (SOAs) are also important components for optical networks. They are very attractive for their wide gain spectrum, and capability of integration with other devices. In the linear regime, they can be used for both booster and in-line amplifiers (O'Mahony, 1988; Settembre et al., 1997; Simon, 1987). Also, much research activities have been done on all-optical signal processing with SOAs (Danielsen et al., 1998; Durhuus et al., 1996). Laser diodes (LDs) are similar devices to SOAs, and they are also the key components for various applications ranging from high-end and high-speed (i.e. fiber communications, and compact-disc players) to low-end and low-speed (i.e. laser pointers, and laser displays) systems. In this chapter, a new unified equivalent circuit model for SOAs and LDs is also presented.

2. Equivalent circuit model for erbium-doped fiber amplifiers

Sun et al. (Sun et al., 1996) derived a nonlinear ordinary differential equation to describe EDFA dynamics. Then, Bononi, Rusch, and Tancevski (Bononi et al., 1997) developed an equivalent circuit model to study EDFA dynamics. Based on this equation, Novak and

Gieske (Novak & Gieske, 2002) also presented a MATLAB Simulink model of EDFA. However, most EDFA models (Barnard et al., 1994; Freeman & Conradi, 1993; Giles et al., 1989; Novak & Gieske, 2002; Novak & Moesle, 2002) didn't take the ASE into account. Some models or methods of EDFA analysis had been presented with ASE (Araci & Kahraman, 2003; Burgmeier et al., 1998; Ko et al., 1994; Wu & Lowery, 1998), but a complex numerical computation was involved in a model or the ASE was simply taken as an independent light source.

Thus, in this section, the Bononi-Rusch-Tancevski model is extended to develop a new equivalent circuit model of EDFAs including ASE. Through the aid of a SPICE simulator, it is convenient to implement the circuit model and to analyze accurately the static and dynamic features of EDFAs.

2.1 Circuit model of EDFA including ASE

Considering a co-pumped two-level EDFA system, it is assumed that the excited-state absorption and the wavelength dependence of group velocity (υ_g) can be ignored. Let the optical beams propagate in z-direction through an EDF of length L. The rate equation and the propagating equations of photon fluxes in time frame can be simplified by transforming to a retarded-time frame moving with υ_g. These equations are shown as

$$\left(\frac{1}{\tau}+\frac{\partial}{\partial t}\right)N_2(z,t)=\sum_{k=p,\,s,\,A}\left[N_t\sigma_k^a-N_2(z,t)\sigma_k^{ae}\right]\Gamma_k P_k(z,t) \tag{1}$$

$$\frac{\partial P_k(z,t)}{\partial z}=\left[\sigma_k^{ae}N_2(z,t)-\sigma_k^a N_t\right]\Gamma_k P_k(z,t) \tag{2}$$

$$\pm\frac{\partial P_{a,l}^{\pm}(z,t)}{\partial z}=\left[\sigma_l^{ae}N_2(z,t)-\sigma_l^a N_t\right]\Gamma_l P_{a,l}^{\pm}(z,t)+\frac{2\Gamma_l\sigma_l^e\Delta\nu_{a,l}}{A}N_2(z,t) \tag{3}$$

where $P_k=P_k'/(h\nu_k A)$, P_k' is the power of the kth optical beam, ν_k is the optical frequency, h is Planck's constant; N_t is the erbium density in the fiber core of effective area A; Γ_k is the overlap factor of the kth beam; τ is the fluorescence lifetime of the metastable level; $\sigma_k^{ae}=\sigma_k^a+\sigma_k^e$, σ_k^a and σ_k^e are respectively the absorption and emission cross sections at the wavelength λ_k; k = p, s, A represent the pump beam (p), signal beam (s), and ASE (A); $P_A(z,t)=P_A^+(z,t)+P_A^-(z,t)=\sum_{l=1}^{m}\left[P_{a,l}^+(z,t)+P_{a,l}^-(z,t)\right]$, m is the number of frequency slots used in the ASE subdivision, $P_{a,l}^+$ and $P_{a,l}^-$ represent the forward and backward ASE fluxes within a frequency slot of width $\Delta\nu_{a,l}$, centered at optical frequency $\nu_{a,l}$ (wavelength $\lambda_{a,l}$). It is noted that s may be replaced by multichannel signals s(1), s(2), …, and s(M).

By Eqs. (1)-(3), the equations can be obtained

$$\left(\frac{1}{\tau_a}+\frac{d}{dt}\right)\bar{N}_2(t)=\sum_{k=s,p,\,A}\left[P_k^{in}(t)-P_k^{out}(t)\right] \tag{4}$$

$$P_{s,p}(z=L,t)=P_{s,p}(z=0,t)G_{s,p}(t) \tag{5}$$

$$P^{\pm}_{a,l}(z=\frac{L\pm L}{2},t)\approx P^{\pm}_{a,l}(z=\frac{L\mp L}{2},t)\left[1+\frac{2\Gamma_l\sigma^e_l\Delta\nu_{a,l}}{A}\int_0^L\frac{N_2(z,t)}{P^{\pm}_{a,l}(z,t)}dz\right]G_l(t) \tag{6}$$

where $\tau_a^{-1}=\tau^{-1}-\sum_{l=1}^{m}4\Gamma_l\sigma^e_l\Delta\nu_{a,l}/A$, $\bar{N}_2(t)=\int_0^L N_2(z,t)dz$, $P^{in}_{s,p}=P_{s,p}(z=0,t)$, $P^{out}_{s,p}=P_{s,p}(z=L,t)$,

$P^{in}_A(t)=\sum_{l=1}^{m}\left[P^+_{a,l}(z=0,t)+P^-_{a,l}(z=L,t)\right]$, $P^{out}_A(t)=\sum_{l=1}^{m}\left[P^+_{a,l}(z=L,t)+P^-_{a,l}(z=0,t)\right]$, and

$G_k(t)=\exp\left\{\Gamma_k\left[\sigma^{ae}_k\bar{N}_2(t)-\sigma^a_kN_tL\right]\right\}$. For simplicity, let an approximation make in this model: $P^{\pm}_{a,l}(z,t)\approx$ constant in Eq. (6) and write

$$P^{\pm}_{a,l}(z=\frac{L\pm L}{2},t)\approx\left[P^{\pm}_{a,l}(z=\frac{L\mp L}{2},t)+\frac{2\Gamma_l\sigma^e_l\Delta\nu_{a,l}}{A}\bar{N}_2(t)\right]G_l(t) \tag{7}$$

In general, the forward ASE remains constant at moderate pump power if the high-gain EDF length is not too long (around 4m in the case of (Pederson et al., 1990)). The forward ASE grows with pump power if the EDF fiber is long. Moreover, for a long EDF fiber (>10m in this case), the growth (or attenuation) of forward ASE along fiber length can not be ignored if the pump power is large (or small). A subdivision of EDF into small segments is necessary in case of long fiber. A similar conclusion holds for the backward ASE. The validity of the approximation of constant ASE power along the EDF will be shown in next subsection.

Subdividing the EDF into n segments with lengths L_i, i = 1, 2, …, n, an equivalent circuit model of EDFA including ASE contributions is developed for Eqs. (4), (5), and (7), as shown in Fig. 1, where $V_{N2,i}=\bar{N}_{2,i}(t)$; the subscript i in the $P^{in(out)}_{s(M),i}$, $P^{in(out)}_{p,i}$, $P^{\pm in(out)}_{A,i}$, or $P^{\pm in(out)}_{SE,i}$ represents the number of EDF segments; $I^{in(out)}_{total,i}=\sum\left(P^{in(out)}_{s(M),i}+P^{in(out)}_{p,i}+P^{\pm in(out)}_{A,i}\right)$; M is the

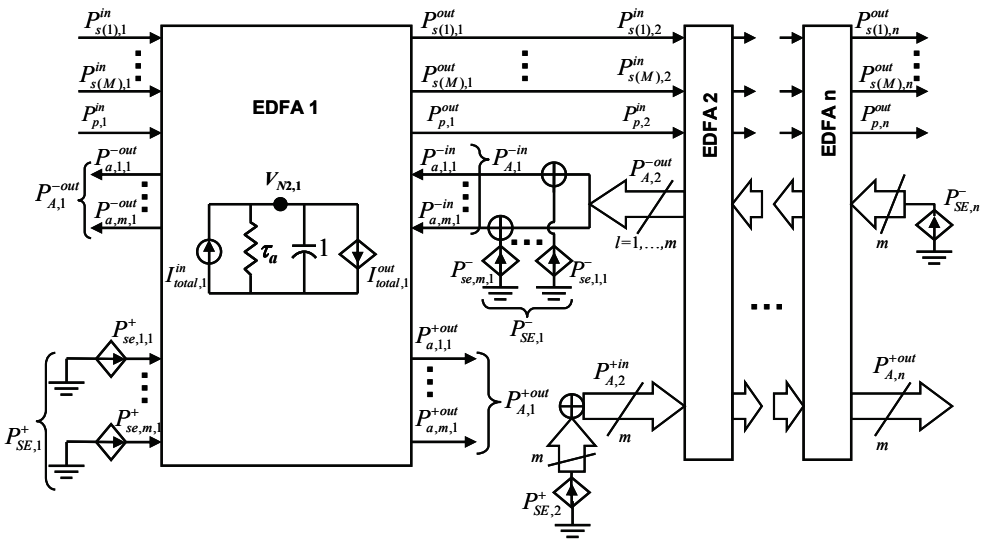

Fig. 1. Equivalent circuit model of EDFA including ASE

number of channels in a multichannel system; $P_{A,i}^{+in} = P_{A,i-1}^{+out} + P_{SE,i}^{+} = \sum_{l=1}^{m}\left(P_{a,l,i-1}^{+out} + P_{se,l,i}^{+}\right)$ with $P_{A,0}^{+out} = 0$; $P_{A,i}^{-in} = P_{A,i+1}^{-out} + P_{SE,i}^{-} = \sum_{l=1}^{m}\left(P_{a,l,i+1}^{-out} + P_{se,l,i}^{-}\right)$ with $P_{A,n+1}^{-out} = 0$; and $P_{se,l,i}^{\pm} = 2\Gamma_l \sigma_l^e \Delta\nu_{a,l} \bar{N}_{2,i} / A$.

2.2 Static gain of EDFA

A forward 980nm-pump EDFA with 12m EDF length and 50μW input signal power at 1558nm are considered. Other parameters used in these simulations are: $N_T = 7.7\times10^{24}m^{-3}$, τ= 10ms, $A = 2.5\times10^{-11}m^2$, $\sigma_s^a = 2.4\times10^{-25}m^2$, $\sigma_s^e = 3.8\times10^{-25}m^2$, $\sigma_p^a = 2.0\times10^{-25}m^2$, and NA = 0.18. These parameters are obtained from manufacturing data or the fitting of experimental gain (Jou et al., 2000; Lai et al., 1999). The dc gain is shown in Fig. 2, as a function of pump power. The square keys represent experimental data (Lai et al., 1999). As a comparison, the numerical calculation is from Eqs. (1)-(3). The numerical results calculated with ASE are shown as the filled circle keys. The EDF length is subdivided into 1200 segments in this numerical computation. The dash curves represent the circuit-model simulation without ASE (Bononi et al., 1997). The solid curve represents the simulation result using this equivalent circuit model. In the circuit models, the parameters used are: the EDF segment number n = 5, the centered wavelength of ASE light λ_a = 1540nm, the bandwidth $\Delta\nu_a$ = 5.06 THz (from 1520nm to 1560nm), and the average cross-section $\sigma_a^e = 5.6\times10^{-25}m^2$ and $\sigma_a^a = 4.8\times10^{-25}m^2$.

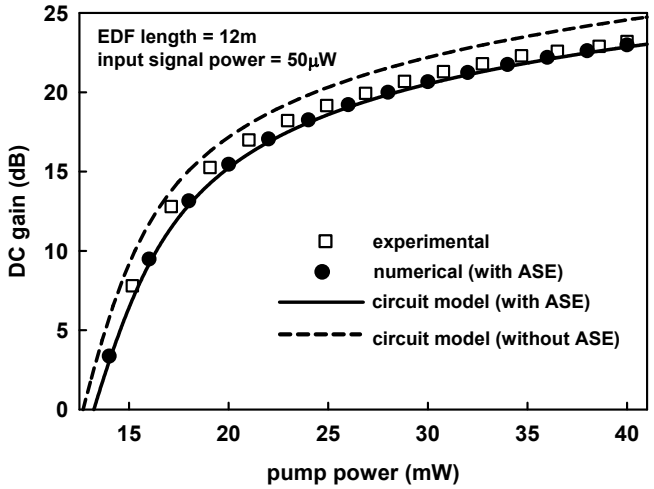

Fig. 2. Measured and simulated dc gain versus pump power for EDFA

Because of the ASE influences on EDFA, the dc gain without ASE is higher than the numerical and circuit-model simulations with ASE. Similar result was also reported by (Novak & Moesle, 2002). In Fig. 2, it is observed that the simulation without ASE results in a dc gain of 2dB lager than the experimental data when the pump power is around 25mW. A good agreement between the measured data and the simulation using this circuit model is obtained. The result of this circuit-model simulation is also in very good agreement with the numerical computation.

Generally, if the EDF is subdivided into more segments, the numerical computation results would be more accurate (Yu & Fan, 1999). However, the circuit model of EDFA without ASE should not be subdivided (Bononi et al., 1997), but the EDF should be subdivided for including ASE in this model. The simulated dc gains of the EDFA are shown in Fig. 3(a), using different number of EDF segments. The dc gain deviation is about 0.2dB between the numerical result using 1200 EDF segments and the circuit-model simulation using 3 EDF segments. Using 5 EDF segments, this simulation can be very close to the numerical result. In Fig. 3(b), the total forward and backward ASE power versus pump power can be shown. It is observed that the forward ASE power is lower than the backward one, since a forward pump EDFA is considered here.

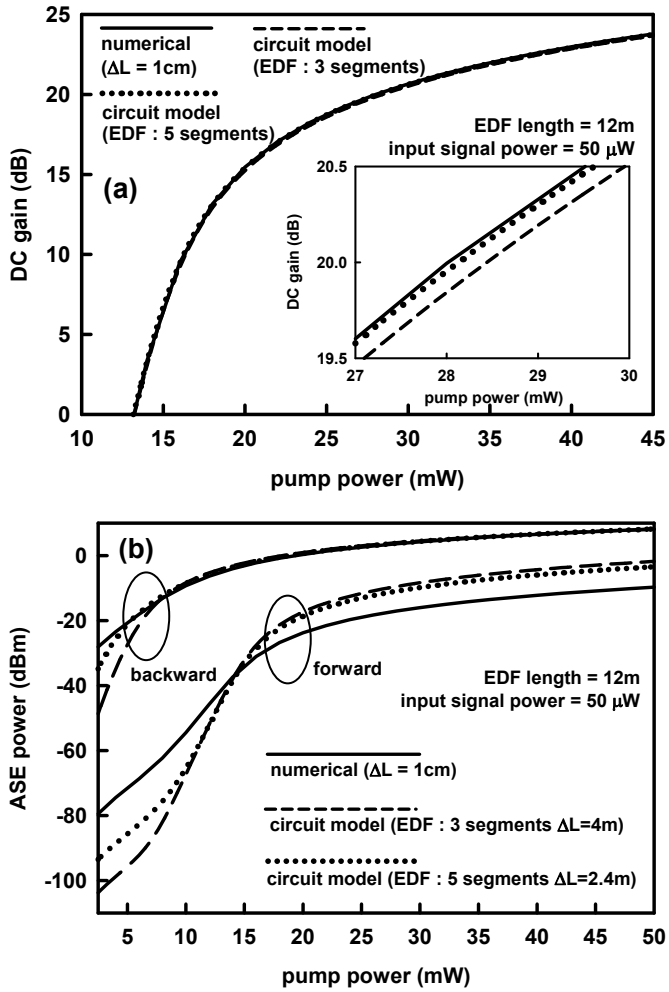

Fig. 3. Static characteristics of EDFA for the different number of subdivided EDF segments (a) DC gain versus pump power (b) ASE power versus pump power

The ASE power of circuit-model simulation is slightly higher than the numerical computation. This makes the dc gain of this circuit-model simulation slightly lower, as expected. When the pump power is around 13mW, the dc gain is around 0dB and the ASE power of circuit-model simulation is in excellent agreement with the numerical computation. The forward ASE power from this circuit model is overestimated when the pump power is above 13mW. This overestimation is believed to be due to this approximation of constant $P_{a,l}^{\pm}(z,t)$ in Eq. (6) and the fact that the forward ASE grows with EDF fiber length in a longer fiber under some given pump power. It is noted that $P_{se,l}^{\pm} = 2\Gamma_l \sigma_l^e \Delta\nu_{a,l} \bar{N}_2(t)/A$ appears in Eq. (7). The use of larger $P_{se,l}^{\pm}$ in this circuit-model simulation can lead to the overestimation of forward ASE, especially in the first and last EDF segments. An improvement in the overestimation is observed using 5-segment EDF instead of 3-segment one, but the model with 5-segment EDF would be more complex. Therefore, the tradeoff between the calculation accuracy and the circuit model complexity should be cautiously considered. Below 13 mW pump power, an underestimation of forward ASE can be found in Fig. 3(b). It is also believed to come from this approximation of constant $P_{a,l}^{\pm}(z,t)$ in Eq. (6) and the attenuation of ASE along EDF fiber. It is noted that the smaller $P_{se,l}^{\pm}$ appears in Eq. (7). A similar conclusion can be reached for the backward ASE. However, the agreement between the backward ASE of this circuit model and the numerical computation is better owing to considering a forward pumped EDFA.

2.3 ASE spectrum of EDFA

An ASE spectrum can also be simulated through this circuit model. It is considered that there are not any input signal beams, the pump power is 55mW, the span of ASE spectrum is from 1520nm to 1560nm, and the cross sections in Fig. 2 of (Desurvire & Simpson, 1989) are used in this simulation. In Figs. 4(a) and 4(b), the numerical results of forward and backward ASE spectra with 40 ASE slots (1nm wavelength spacing) are shown as the filled circle keys. Using this circuit model with 1, 3, and 5 ASE slots, the simulation results are shown as the dotted, dash, and solid curves respectively. The stepped ASE spectrum with 5 ASE slots is coarsely similar to the numerical calculation. Although the stepped ASE spectra using 1 and 3 ASE slots are unlike with the numerical calculation, each total ASE power of those spectra is very similar. If the ASE is subdivided into more slots in this circuit-model simulation, the ASE spectrum would be more accurate, but the model would also become more complex. However, the rough spectra of circuit-model simulations are still worthwhile in the estimation of EDFA's characteristics. In Fig. 4(a), it can also be obtained that the forward ASE power of this circuit model simulation is slightly higher than that of the numerical computation, as the result in Fig. 3(b).

2.4 Frequency response of EDFA

Using this circuit model with ASE, the frequency response of EDFA is also analyzed. The 10% signal power modulation index is used in these ac analyses. When the input pump power is 40mW, the ac gain and phase responses are shown in Figs. 5(a) and 5(b), as a function of frequency. The numerical computation is in a good agreement with this circuit-model simulation and the ac gain response shows a high-pass characteristic (Freeman & Conradi, 1993; Liu et al., 1995; Novak & Gieske, 2002; Novak & Moesle, 2002). When the modulation frequency is below 100Hz, the maximum ac gain deviation can be near 10dB between the simulation results with and without ASE. The peak phase of simulation

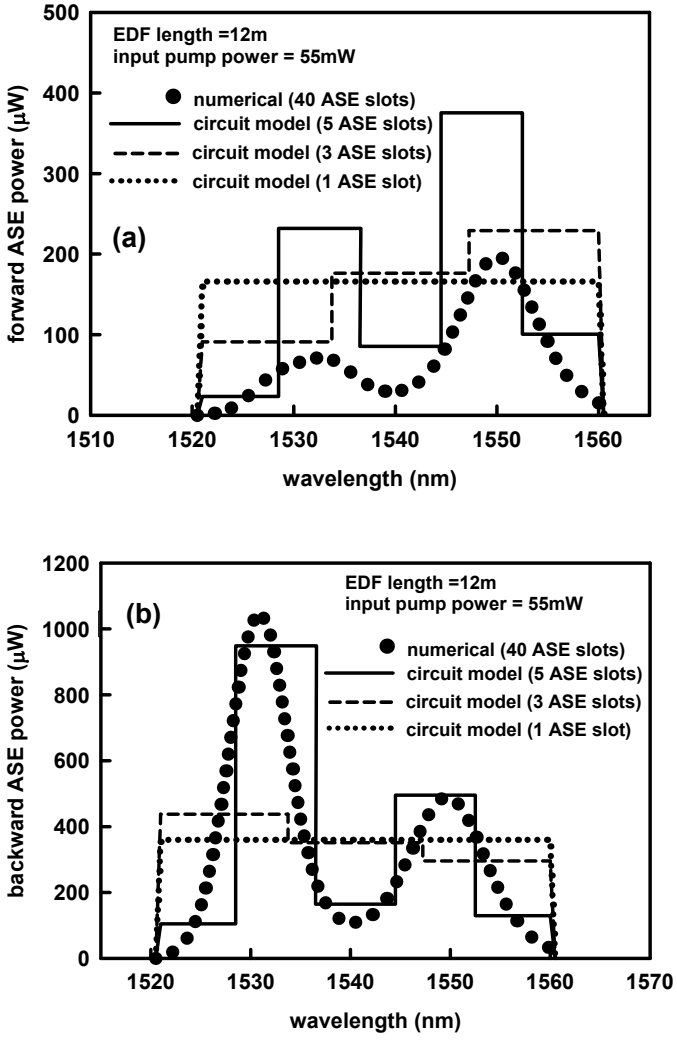

Fig. 4. ASE spectra of EDFA (a) Forward ASE spectrum (b) Backward ASE spectrum

without ASE is about 70 degree at 100Hz. With ASE it is about 30 degree at 230Hz. The deviation of peak phase between the results with and without ASE is quite large. The peak phase position shifts to higher frequency when the simulation includes ASE. The influence of ASE on frequency response of EDFA is significant in low modulation frequency region (below 100Hz). The dc gain of the numerical computation is slightly higher than that of the circuit-model simulation in Fig. 3(a), so the ac gain of the numerical computation is also slightly higher than that of this simulation in low modulation frequency region.

After the numerical computation of transient analysis from Eqs. (1)-(3), the ac gain and phase can be estimated or calculated as functions of frequency. This computing process is more

complex. However, using the circuit model, the frequency response of EDFA can be obtained easily and rapidly by the frequency-sweep analysis command in a SPICE simulator.

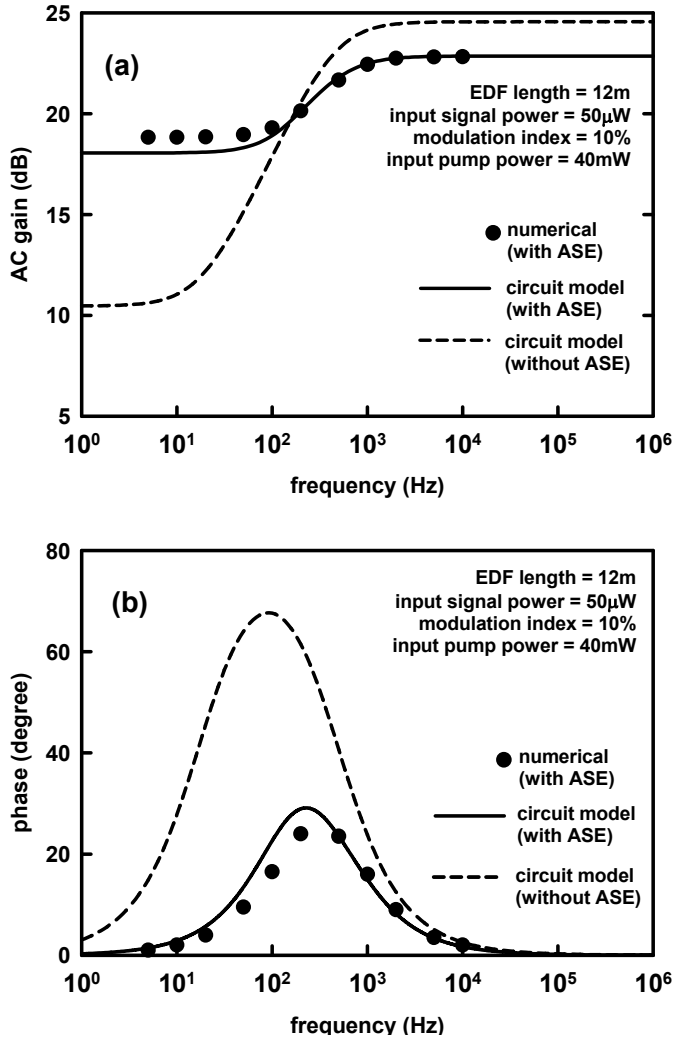

Fig. 5. Frequency responses of EDFA (a) AC gain response (b) Phase response

2.5 Transient analysis of EDFA

Using this circuit model with ASE, the transient response of EDFA dynamics can also be obtained readily through the aid of a SPICE simulator. An eight-channel EDFA system with 35mW pump power at 980nm is considered and seven out of eight channels are added and dropped. These seven channels are represented by a 1558nm signal, while the surviving channel by a 1530nm signal, as shown in Fig. 6(a). (This system can also be regarded as a

two-channel system.) $\sigma_s^a = 8.5\times10^{-25}m^2$ and $\sigma_s^e = 8.1\times10^{-25}m^2$ at 1530nm are used in this simulation. Each channel has 10μW power input to the EDFA. In Fig. 6(b), it is shown that the 1558nm output signal has a large power excursion (Giles et al., 1989; Ko et al., 1994; Wu & Lowery, 1998), when the input signals of seven channels are added simultaneously. According to the above-mentioned results, the dc gain is lower and the ac gain deviation between high and low frequency is smaller, because of the ASE influence on EDFA. Therefore, the power excursion of the transient response is lower in this simulation with ASE, as shown by the features in Fig. 6(b). A good agreement between the numerical computation and this circuit-model simulation is obtained.

When the 1558nm signal is added or dropped, the output power of 1530nm surviving channel can decrease or increase due to the effect of cross talk, as shown in Fig. 6(c). Because of the ASE influence on EDFA, the 1530nm output power of the simulation without ASE is higher, and that of the numerical computation is also slightly higher than that of the circuit-model simulation with ASE. A larger difference between the result of the numerical computation and this circuit-model simulation can be observed when the 1558nm signal is

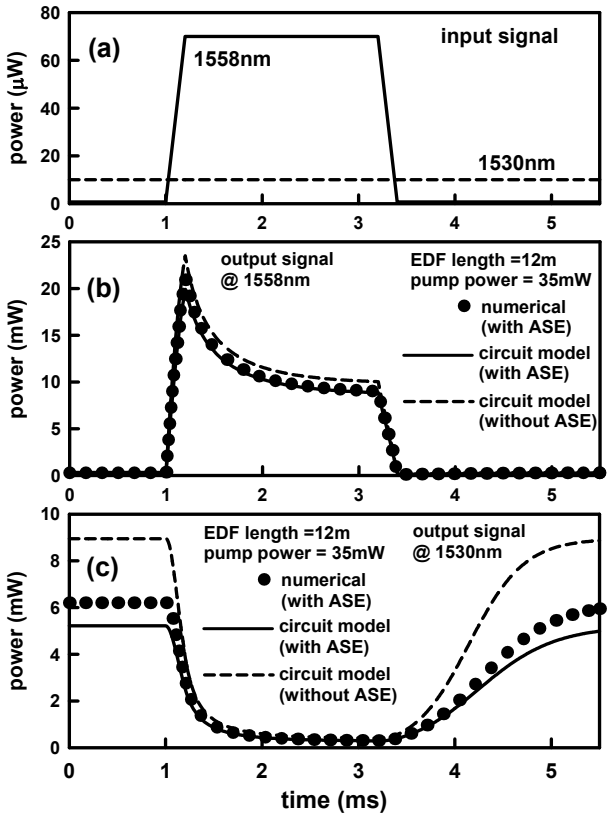

Fig. 6. Transient responses of a two-channel EDFA system (a) Input signals (b) Output signal at 1558nm (c) Output signal at 1530nm

dropped. However, the agreement between this circuit model and the numerical computation is better when the 1558nm signal is added.
To include the forward and backward ASE in a transient analysis, the iteration process in the two-point boundary-value problem gets complex. The numerical simulation requires a large amount of computation time and dynamic data storage, and the convergence problem is not easy to deal with. However, using the circuit model, the transient response of EDFA can be obtained conveniently through the aid of a SPICE simulator. Setting a given tolerance criteria and the number of iterations in a SPICE simulator, the convergence problem can be solved easily and the computer time can also be reduced (Avant!, 2001).

3. Unified circuit model for semiconductor optical amplifiers and laser diodes

There are two primary types of SOAs: traveling wave (TW) SOAs and Fabry-Perot (FP) SOAs. The principle of TW-SOA and FP-SOA is identical, i.e. intrinsic stimulated light amplification. The difference between TW-SOA and FP-SOA is reflectivity of cavity facets. The internal reflectivity of FP-SOA is higher than TW-SOA. Actually, an FP-SOA can be regarded as a FP-LD that is biased below the threshold current. The active layer of an SOA has a positive medium gain but not large enough for laser emission.
Equivalent circuit models have been separately reported for LDs (Lu et al., 1995; Rossi et al., 1998; Tsou & Pulfrey, 1997) and SOAs (Chen et al., 2000; Chu & Ghafouri-Shiraz, 1994; Sharaiha & Guegan, 2000). However, the principles of SOAs and LDs are extremely similar. In this section, a unified equivalent circuit model is presented for SOAs and LDs.

3.1 Circuit model of SOA and LD

Schematic diagrams of a TW-SOA and an FP-SOA are shown in Fig.7 (a) and (b), respectively. TW-SOAs are of a very low internal reflectivity and the incident light is amplified in single pass. FP-SOAs are of a higher reflectivity and incident light can be bounced back and forth within the cavity, resulting in resonance amplification. A basic LD structure is similar to an FP-SOA, but it doesn't need any incident light.
Assume that the nonradiative recombination and carrier leakage rate can be neglected; the wavelength dependence of group velocity (υ_g) can be ignored; any transport time for carriers to reach the active region is not considered. The rate equation for carrier density N, and the continuity equations for signal photon $N^{\pm}_p$ and ASE photon $N^{\pm}_{sp}$ propagating in ±z-direction can be written as (Coldren & Corzine, 1995)

$$\frac{\partial N}{\partial t'} = \frac{\eta_i I}{qV} - R_{sp}(N) - \upsilon_g\left[g_m(N_p^+ + N_p^-) + \langle g_m\rangle\left(N_{sp}^+ + N_{sp}^-\right)\right] \tag{8}$$

$$\frac{1}{\upsilon_g}\frac{\partial N_p^{\pm}}{\partial t'} \pm \frac{\partial N_p^{\pm}}{\partial z'} = \Gamma g_m N_p^{\pm} - \alpha_i N_p^{\pm} \tag{9}$$

$$\frac{1}{\upsilon_g}\frac{\partial N_{sp}^{\pm}}{\partial t'} \pm \frac{\partial N_{sp}^{\pm}}{\partial z'} = \Gamma\langle g_m\rangle N_{sp}^{\pm} - \langle\alpha_i\rangle N_{sp}^{\pm} + \Gamma\frac{\beta_{sp}}{\upsilon_g}R_{sp} \tag{10}$$

where η_i is the internal quantum efficiency, I is the injected current, V is the volume of the active region, Γ is the confinement factor, $R_{sp}(N)$ is the spontaneous emission rate,

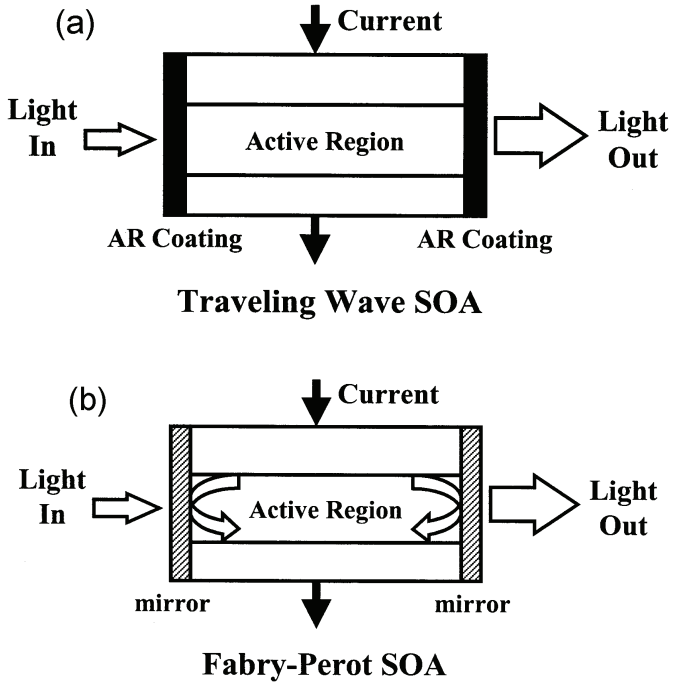

Fig. 7. Schematic diagrams of (a) TW-SOA and (b) FP-SOA

$g_m\left(\approx a\left(N-N_0\right)\right)$ is the material gain, a is the differential gain, N_0 is the transparency carrier density, α_i is the internal loss, and β_{sp} is the spontaneous emission factor. $\langle g_m\rangle$ and $\langle\alpha_i\rangle$ are the spectral average material gain and internal loss over ASE spectrum, respectively. The equations can be simplified by transforming to a retarded-time frame moving with velocity υ_g, $t = t' - z/\upsilon_g$, and $z = z'$. Eqs. (9) and (10) can be written as

$$\pm\frac{\partial N_p^{\pm}}{\partial z} = \Gamma g_m N_p^{\pm} - \alpha_i N_p^{\pm} \tag{11}$$

$$\pm\frac{\partial N_{sp}^{\pm}}{\partial z} = \Gamma\langle g_m\rangle N_{sp}^{\pm} - \langle\alpha_i\rangle N_{sp}^{\pm} + \Gamma\frac{\beta_{sp}}{\upsilon_g}R_{sp} \tag{12}$$

Eqs. (11) and (12) are integrated over z from 0 to the length of active region L. The photon $N_p^{\pm}$ and $N_{sp}^{\pm}$ can be transformed into the signal power $P_s^{\pm}$ and the ASE average power $P_{sp}^{\pm}$, respectively. Then, by Eqs. (8), (11), and (12), these equations are shown as

$$\frac{\partial N}{\partial t} \approx \frac{\eta_i I}{qV} - R_{sp} - \frac{\Gamma g_m}{h\nu_s A_s g_s}\left(\frac{\partial P_s^{+}}{\partial z} - \frac{\partial P_s^{-}}{\partial z}\right) - \frac{\Gamma\langle g_m\rangle}{h\nu_s A_s\langle g_s\rangle}\left(\frac{\partial P_{sp}^{+}}{\partial z} - \frac{\partial P_{sp}^{-}}{\partial z}\right) \tag{13}$$

$$P_s^{\pm}(z=\frac{L\pm L}{2})=P_s^{\pm}(z=\frac{L\mp L}{2})\exp\left(\int_0^L g_s dz\right) \tag{14}$$

$$P_{sp}^{\pm}(z=\frac{L\pm L}{2})=P_{sp}^{\pm}(z=\frac{L\mp L}{2})\exp\left(\int_0^L \langle g_s\rangle dz+\beta_{sp}h\nu_{sp}A_s\int_0^L\frac{R_{sp}}{P_{sp}^{\pm}}dz\right) \tag{15}$$

where $g_s = (\Gamma g_m - \alpha_i)$, h is the Plank's constant, ν_s is the signal frequency, ν_{sp} is the ASE central frequency, A_s is the cross-section area of the active region in z-direction. Assume that the distribution of carrier density N approximates a constant in z-direction and $P_{sp}^{\pm}(z)\approx P_{sp}^{\pm}(z=\frac{L\mp L}{2})\exp\left(\langle g_s\rangle z\right)$. Eq. (13) is integrated over z from 0 to L. These equations are shown as

$$\begin{aligned} q\frac{\partial N_T}{\partial t}\approx{}&\eta_i I-qVR_{sp}-\frac{q\Gamma g_m}{h\nu_s g_s}\left[\left(P_s^{+out}+P_s^{-out}\right)-\left(P_s^{+in}+P_s^{-in}\right)\right]\\ &-\frac{q\Gamma\langle g_m\rangle}{h\nu_{sp}\langle g_s\rangle}\left[\left(P_{sp}^{+out}+P_{sp}^{-out}\right)-\left(P_{sp}^{+in}+P_{sp}^{-in}\right)\right]\end{aligned} \tag{16}$$

$$P_s^{\pm out}\approx P_s^{\pm in}G_s \tag{17}$$

$$P_{sp}^{\pm out}\approx\left(P_{sp}^{\pm in}+\beta_{sp}h\nu_{sp}A_sR_{sp}\frac{\langle G_s\rangle-1}{\langle g_s\rangle\langle G_s\rangle}\right)\langle G_s\rangle=\left(P_{sp}^{\pm in}+P_{sp0}\right)\langle G_s\rangle \tag{18}$$

where N_T is the total carriers in the active region, $G_s=\exp\left(g_sL\right)$, $P_{s(sp)}^{\pm in}=P_{s(sp)}^{\pm}(z=\frac{L\mp L}{2})$, and $P_{s(sp)}^{\pm out}=P_{s(sp)}^{\pm}(z=\frac{L\pm L}{2})$.

The principles of FP-SOA, TW-SOA, and LD are identical, but their boundary conditions are different. The boundary conditions can be considered: 1) FP-SOA: at z = 0, $P_s^{+in}=\left(\sqrt{(1-R)P_{signal}^{in}}+\sqrt{RP_s^{-out}}\right)^2$, where P_{signal}^{in} is the incident signal light power, and $P_{sp}^{+in}=RP_{sp}^{-out}$; at z = L, $P_{s(sp)}^{-in}=RP_{s(sp)}^{+out}$, and $P_{signal}^{out}=(1-R)P_s^{+out}$, where P_{signal}^{out} is the amplified signal output power. 2) TW-SOA: the reflectivity of facets R = 0, $P_s^{-in(out)}=0$, $P_s^{+in}=P_{signal}^{in}$, and $P_{signal}^{out}=P_s^{+out}$. 3) Laser: no incident signal, $P_s^{\pm in(out)}=0$, $P_{sp}^{\pm in}=RP_{sp}^{\mp out}$, and $P_{signal}^{\pm out}=(1-R)P_{sp}^{\pm out}$, where $P_{signal}^{\pm out}$ is laser output power in ±z-direction. A unified equivalent circuit model of SOA and LD is developed for the Eqs. (16)-(18), as shown in Fig. 8, where $V_{Nt} = qVR_{sp}$, $E_{Nt}(V_{Nt}) = N_T(R_{sp})$, $P_{s,total}^{in(out)}=g_k\left(P_s^{+in(out)}+P_s^{-in(out)}\right)$, $P_{sp,total}^{in(out)}=\langle g_k\rangle\left(P_{sp}^{+in(out)}+P_{sp}^{-in(out)}\right)$, and $g_k=q\Gamma g_m/\left(h\nu_s g_s\right)$. Lossless transmission lines are employed with time delay $\Delta = L/\upsilon_g$ from light beams propagating. Using this circuit model and suitable boundary conditions, the performances of SOA and LD can be analyzed and simulated.

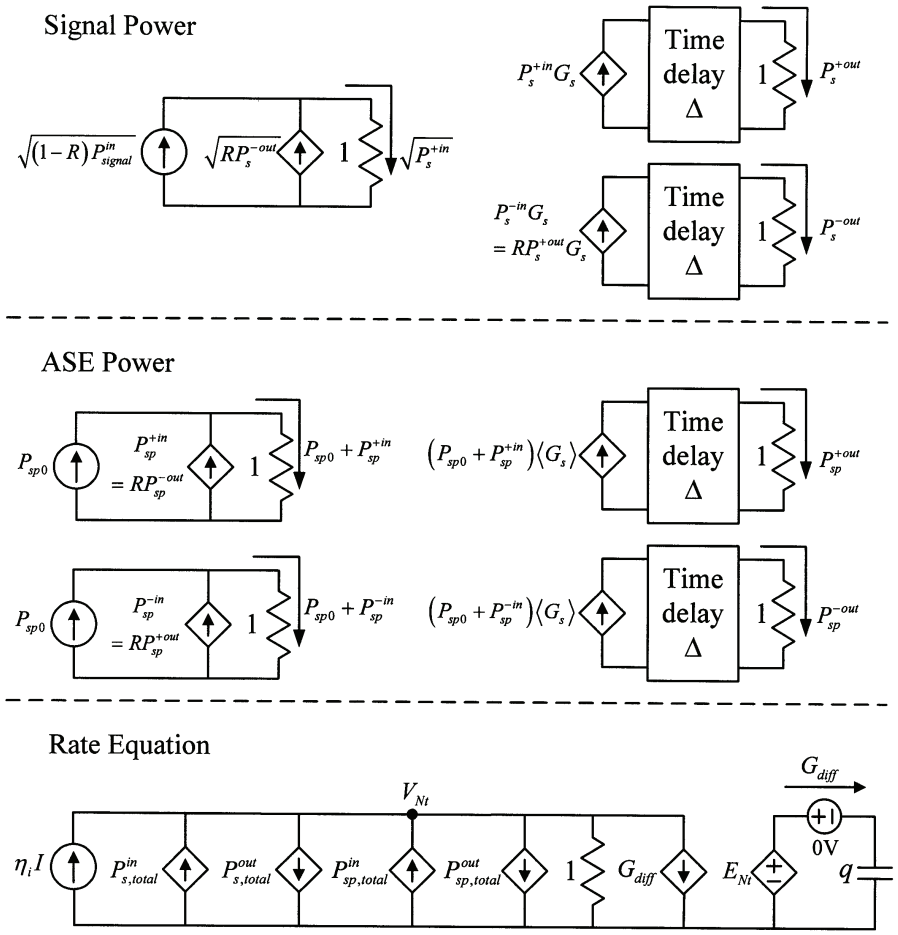

Fig. 8. A unified equivalent circuit model of SOA and LD

3.2 Model validation and analysis of SOA

To demonstrate the validity of this model, the gain against input signal power is simulated for SOAs. First, it is considered the TW-SOA having $R_{sp} = N/\tau_{sp} = (N_T/V)/\tau_{sp}$, τ_{sp} is the spontaneous carrier lifetime. With τ_{sp} = 4ns, η_i = 1, R = 0, Γ = 0.5, a = 5×10^{-16}cm^2, N_0 = 10^{18}cm^{-3}, L = 200μm, A_s = 0.3μm^2, V = 60μm^3, $h\nu_s$ = 0.8eV, υ_g = 0.75×10^8m/s, α_i = 0cm^{-1}, and β_{sp} = 0 (Adams et al., 1985), the results of the TW-SOA without ASE are shown in Fig. 9. It can be shown as expected that the gain of TW-SOAs becomes higher when the higher current injects or the lower signal light power inputs to the SOA. In Fig. 9, with the 3mA injection current and the -60dBm to -20dBm input signal power, the gain of TW-SOAs is fixed about 5.4dB. The influence of input signal power on gain becomes obvious when the higher current injects. These simulations are shown as the solid curves. The results of Ref. (Adams et al., 1985) are shown as the circle keys. A good agreement between this simulation and Ref. (Adams et al., 1985) is observed.

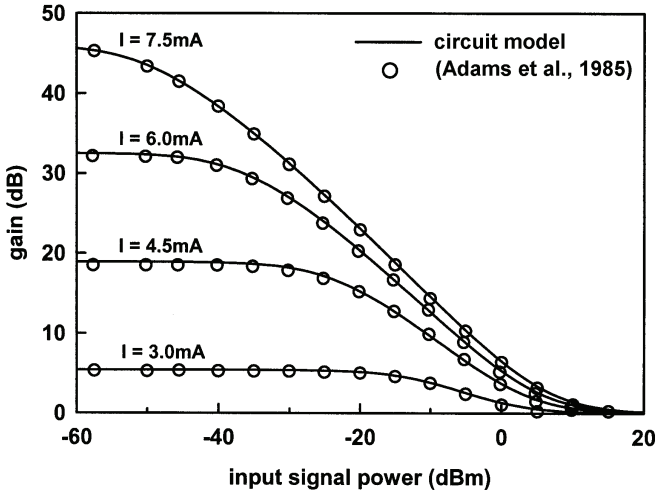

Fig. 9. Gain against input signal power for TW-SOA

Next, it is considered the FP-SOA having $R_{sp} = BN^2 = B\left(N_T/V\right)^2$, B is the bimolecular recombination coefficient. The same parameters are used in the first example except R = 0.01, B = 10^{-10}cm^3/s, α_i =25cm^{-1}, β_{sp} = 10^{-4} (Adams et al., 1985), and the threshold current $I_{th} \approx 3.93$mA can be obtained. FP-SOAs must be biased below the threshold current. In Fig. 4, the $0.99I_{th}$, $0.95I_{th}$ and $0.9I_{th}$ injection currents are used, and the results of the FP-SOA without and with ASE are shown in Fig. 10(a) and (b), respectively. Similar to the TW-SOA, the gain of FP-SOAs becomes higher when the injection current more tends to the threshold current or the lower signal light power inputs to the SOA. In Fig. 10(b), it can be observed that the degeneration of the gain of FP-SOAs is influenced by ASE, it becomes more obvious when the injection current tends to the threshold current. These simulations (solid curves) are in good agreement with Ref. (Adams et al., 1985) (circle keys). The agreement can indicate the validity of this model for TW-SOA and FP-SOA.

In this simplified model shown above, the non-uniformity of carrier density is neglected. In fact, the carrier density is non-uniform along the SOA active region. In this simplified SOA model, the rate equation for spatially averaged values of carrier density is used, and the simulation results of gain are slightly high in comparison with a real SOA (Giuliani & D'Alessandro, 2000). However, the simplified model can be helpful for the coarse definition of SOA's parameters. More accurate results can be obtained by the method of cascading, i.e., by subdividing the SOA into many longitudinal sections and using a simplified model with uniform carrier density for each section (Giuliani & D'Alessandro, 2000). In this simulation, the SOA can be also divided into many sections, and the circuit model as Fig. 8 can be used for each section, as done in the multi-section circuit model of fiber lasers (Liu et al., 2002). However, the tradeoff between the result accuracy and the model complexity should be considered.

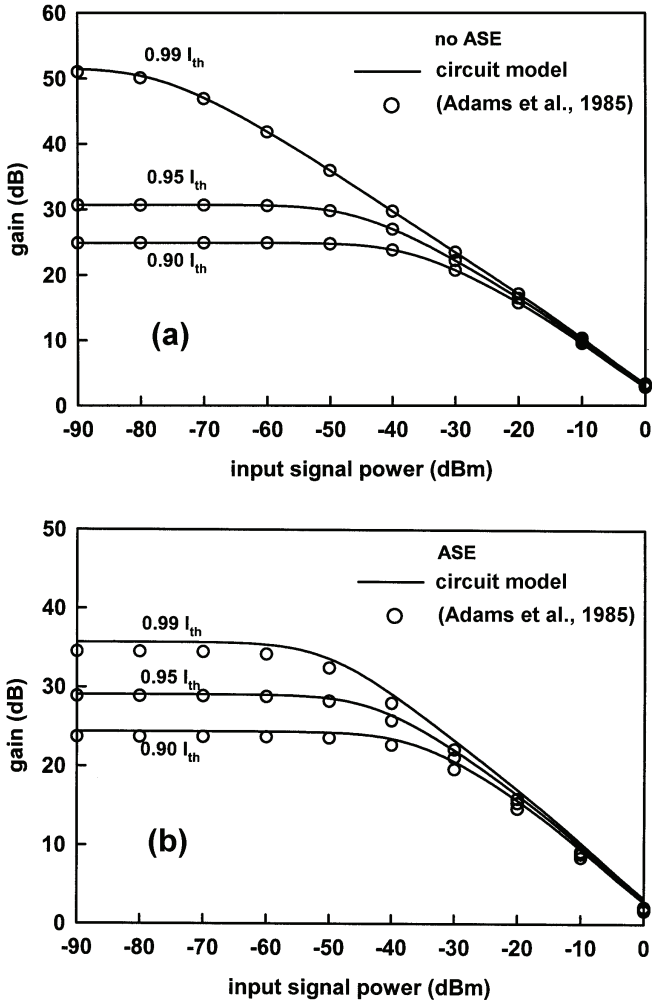

Fig. 10. Gain against input signal power for FP-SOA (a) without ASE and (b) with ASE

3.3 Static and dynamic analysis of laser diode

Then, the characteristics of LD are also analyzed by this model. The parameters used are the same as those of the above example for the FP-SOA. The light output power against injection dc current is simulated for laser diodes having different reflectivity of facets and the results are shown in Fig. 11(a). The higher reflectivity of facets is, and the lower threshold current of the laser is. The threshold current can be expressed as (Liu, 1996),

$$I_{th} = \frac{1}{\eta_i} qVR_{sp}(N_{th}) \tag{19}$$

where $N_{th} = N_0 + \alpha_{tot}/(\Gamma a)$ and $\alpha_{tot} = \alpha_i - (\ln R)/L$. The threshold current versus reflectivity of facets is shown in Fig. 11(b). The circle keys and the solid curve represent, respectively, these simulations and the results of Eq. (19), and the results of the both methods are agreeable.

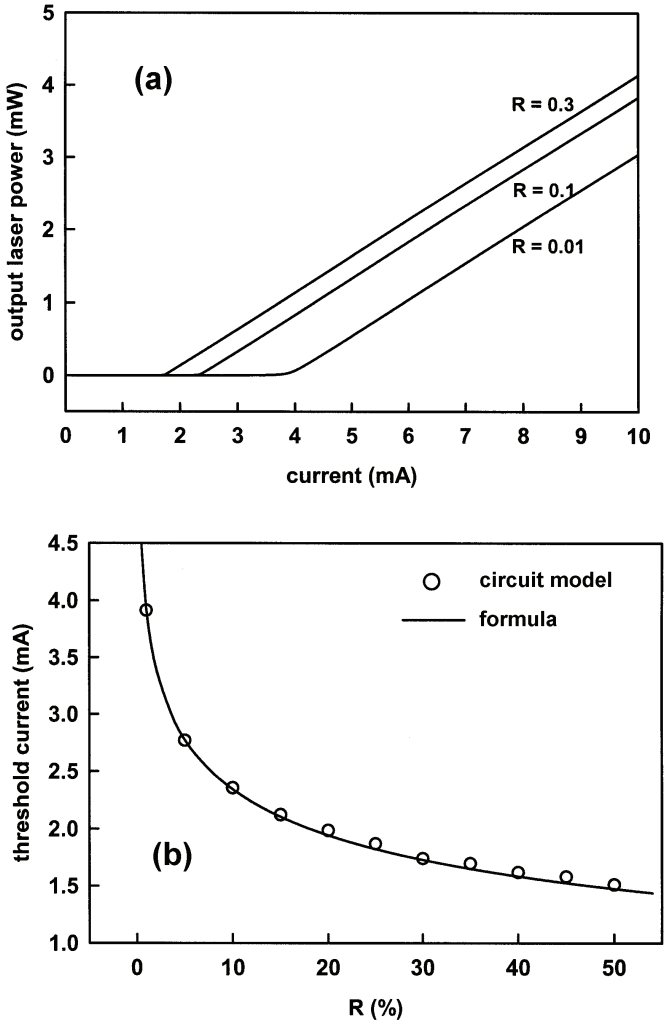

Fig. 11. (a) L-I curve of LDs and (b) the threshold current vs. reflectivity of facets

In Fig. 12 (a), the frequency responses of the laser diode are shown using this circuit model. The 10% current modulation index is used in these ac analyses. The responses have different peak values at different bias currents. When the bias current becomes higher, the peak frequency becomes also higher. The peak frequency can be written as (Liu, 1996),

$$f_p = \frac{1}{2\pi}\left[\upsilon_g \alpha_{tot} \frac{R_{sp}(N_{th})}{N_{th}} \frac{I/I_{th} - 1}{1 - N_0/N_{th}}\right]^{0.5} \tag{20}$$

The peak frequency as a function of bias current is shown in Fig. 12(b). The circle keys exhibit these simulations and the results of Eq. (20) are represented by the solid curve. These simulations are in good agreement with the results of this formula.

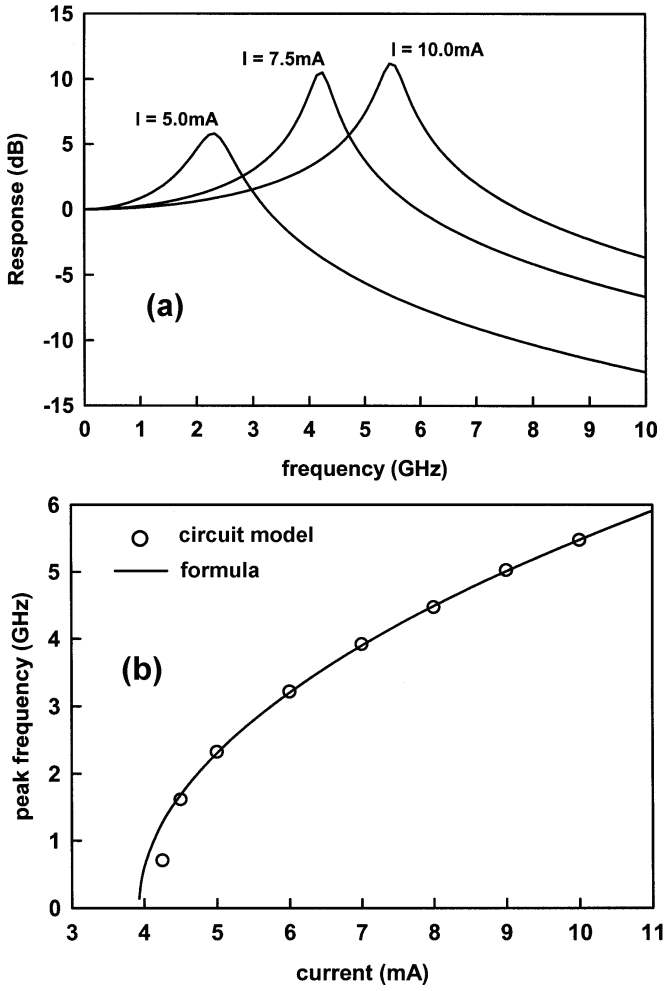

Fig. 12. (a) Frequency responses of LDs and (b) the peak frequency vs. bias current

The transient responses of laser diodes are analyzed during the switching of current. The feature of relaxation oscillation and turn-on delay can be observed in this simulation, as shown in Fig. 13(a). When the turn-on current is higher, the relaxation frequency becomes higher and turn-on delay time is shorter. The turn-on delay time and the relaxation frequency can be formularized as (Liu, 1996),

$$t_d = \frac{N_{th}}{R_{sp}(N_{th})} \frac{\eta_i I/(qV)}{\eta_i I/(qV) - R_{sp}(N_{th})} \tag{21}$$

$$f_r = \frac{1}{2\pi}\sqrt{(2\pi f_p)^2 - \alpha^2} \tag{22}$$

where $\alpha = \frac{1}{2}\frac{dR_{sp}}{dN}\Big|_{N=N_{th}} + \frac{1}{2}\upsilon_g \alpha_{tot} (2\pi f_p)^2$. As shown in Fig. 13(b), the circle keys and the square keys represent these simulations for the turn-on delay time and the relaxation frequency, respectively. The solid curves are the results of Eqs. (21) and (22). These simulations are in agreement with the results of the formulas.

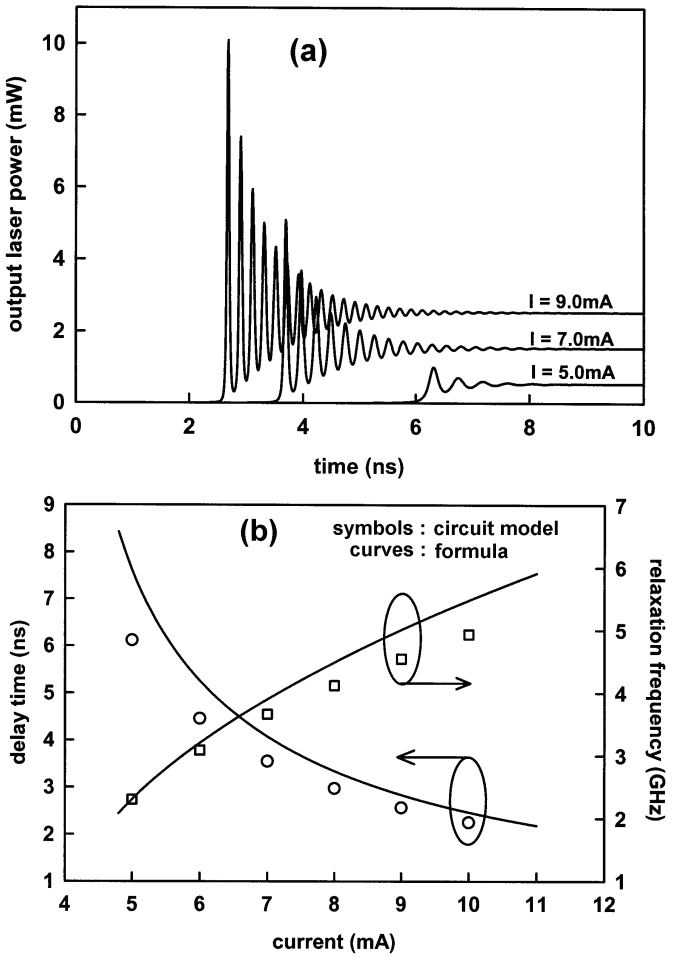

Fig. 13. (a) Transient responses of LDs, and (b) the turn-on delay time and the relaxation frequency vs. bias current

4. Conclusions

An equivalent circuit model of EDFA including ASE is developed. A good agreement between the measured data and this simulation is obtained in the static gain analysis of EDFA. A rough ASE spectrum of EDFA can also be simulated. Furthermore, these simulation results are also in agreement with the numerical computations in the dynamic gain analysis of EDFA. The transient response analyses of a two-channel EDFA system using this circuit model have been demonstrated. Moreover, this circuit model can also be extended to simulate the multichannel, backward-pump, or bidirectional-pump EDFA systems. Besides, this approach could also be applied to develop other numerical model or Simulink model of EDFAs including ASE.

A unified equivalent circuit model of semiconductor optical amplifiers and laser diodes is proposed. The model has been verified by analyzing 1) the gain against input signal power in FP-SOAs and TW-SOAs and 2) the L-I curve, small signal response, and pulse response in laser diodes. The simulation results of this model showed a good agreement with the published results.

Through the aid of SPICE circuit simulator, it is convenient to implement these circuit models. These equivalent circuit models of optical amplifiers can be also extended to include other effects or devices such as modulators, fibers, multiplexers, and parasitic components. The circuit models may be of great value for integrated circuit designers requiring an equivalent circuit model for the amplifiers of the optical communication systems in order to simulate accurately the mixed photonic/electronic modules.

5. References

Adams, M. J.; Collins, J. V. & Henning, I. D. (1985). Analysis of semiconductor laser optical amplifier. *IEE Proc. J. Optoelectron.*, Vol. 132, No. 1, Feb. 1985, pp. 58-63, ISSN 0267-3932

Araci, I. E. & Kahraman, G. (2003). Performance failure analysis of EDFA cascades in optical DWDM packet-switched networks. *J. Lightwave Technol.*, Vol. 21, No. 5, May 2003, pp. 1156-1163, ISSN 0733-8724

Avant! (2001). *Star-Hspice Manual Release 2001.2*, Avant! Corporation

Barnard, C.; Myslinski, P.; Chrostowski, J. & Kavehrad, M. (1994). Analytical model for rare-earth-doped fiber amplifiers and lasers. *IEEE J. Quantum Electron.*, Vol. 30, No. 8, Aug. 1994, pp. 1817-1830, ISSN 0018-9197

Bononi, A.; Rusch, L. A. & Tancevski, L. (1997). Simple dynamic model of fibre amplifiers and equivalent electrical circuit. *Electron. Lett.*, Vol. 33, No. 22, Oct. 1997, pp.1887-1888, ISSN 0013-5194

Burgmeier, J.; Cords, A.; Marz, R.; Schaffer, C. & Stummer, B. (1998). A block box model of EDFAs operating in WDM systems. *J. Lightwave Technol.*, Vol. 16, No. 7, Jul. 1998, pp. 1271-1275, ISSN 0733-8724

Chen, W.; Wang, A.; Zhang, Y., Liu; C. & Liu, S. (2000). Circuit model for traveling wave semiconductor laser. *Solid-State Electron.*, Vol. 44, No. 6, Jun. 2000, pp. 1009-1012, ISSN 0038-1101

Chu, C. Y. J. & Ghafouri-Shiraz, H. (1994). Equivalent circuit theory of spontaneous emission power in semiconductor laser optical amplifiers. *J. Lightwave Technol.*, Vol. 12, No. 5, May 1994, pp. 760-767, ISSN 0733-8724

Coldren, L. A. & Corzine, S. W. (1995). *Diode Lasers and Photonic Integrated Circuit*, John Wiley & Sons, ISBN 978-0471118756, New York

Danielsen, S. L.; Hansen, P. B. & Stubkjaer, K. E. (1998). Wavelength Conversion in Optical Packet Switching. *J. Lightwave Technol.*, Vol. 16, No. 12, Dec. 1998, pp. 2095-2108, ISSN 0733-8724

Desai, N. R.; Hoang, K. V. & Sonek, G. J. (1993). Applications of PSPICE simulation software to the study of optoelectronic integrated circuits and devices. *IEEE Trans. Educ.*, Vol. 36, NO. 4, Nov. 1993, pp. 357-362, ISSN 0018-9359

Desurvire, E. & Simpson, J. R. (1989). Amplification of spontaneous emission in erbium-doped single-mode fibers. *J. Lightwave Technol.*, Vol. 7, No. 5, May 1989, pp. 835-845, ISSN 0733-8724

Durhuus, T.; Mikkelsen, B.; Joergensen, C.; Danielsen, S. L. & Stubkjaer, K. E. (1996). All-optical wavelength conversion by semiconductor optical amplifiers. *J. Lightwave Technol.*, Vol. 14, No. 6, Jun. 1996, pp. 942-954, ISSN 0733-8724

Freeman, J. & Conradi, J. (1993). Gain modulation response of erbium-doped fiber amplifiers. *IEEE Photon. Technol. Lett.*, Vol. 5, No. 2, Feb. 1993, pp. 224-226, ISSN 1041-1135

Giles, C. R.; Desurvire, E. & Simpson, J. R. (1989). Transient gain and cross talk in erbium-doped fiber amplifiers. *Opt. Lett.*, Vol. 14, No. 16, Aug. 1989, pp. 880-882, ISSN 0146-9592

Giuliani, G. & D'Alessandro, D. (2000). Noise analysis of conventional and gain-clamped semiconductor optical amplifiers. *J. Lightwave Technol.*, Vol. 18, No. 9, Sep. 2000, pp. 1256-1263, ISSN 0733-8724

Jou, J.-J.; Lai, F.-S.; Chen, B.-H. & Liu, C.-K. (2000). On-line extraction of parameters in erbium-doped fiber amplifiers. *J. Chinese Ins. Eng.*, Vol. 23, No. 5, Sep. 2000, pp. 615-623, ISSN 0253-3839

Jou, J.-J.; Liu, C.-K.; Hsiao, C.-M.; Lin, H.-H. & Lee, H.-C. (2002). Time-delay circuit model of high-speed p-i-n photodiodes. *IEEE Photon. Technol. Lett.*, Vol. 14, No. 4, Apr. 2002, pp. 525-527, ISSN 1041-1135

Ko, K. Y.; Demokan, M. S. & Tam, H. Y. (1994). Transient analysis of erbium-doped fiber amplifiers. *IEEE Photon. Technol. Lett.*, Vol. 6, No. 12, Dec. 1994, pp. 1436-1438, ISSN 1041-1135

Lai, F.-S.; Jou, J.-J. & Liu, C.-K. (1999). Indicator of amplified spontaneous emission in erbium doped fiber amplifiers. *Elecrton. Lett.*, Vol. 35, No. 7, Apr. 1999, pp. 587-588, ISSN 0013-5194

Liu, C.-K.; Jou, J.-J. & Lai, F.-S. (1995). Second-order harmonic distortion and optimal fiber length in erbium-doped fiber amplifiers. *IEEE Photon. Technol. Lett.*, Vol. 7, No. 12, Dec. 1995, pp. 1412-1414, ISSN 1041-1135

Liu, C.-K.; Jou, J.-J.; Liaw, S.-K. & Lee, H.-C. (2002). Computer-aided analysis of transients in fiber lasers and gain-clamped fiber amplifiers in ring and line configurations

through a circuit simulator. *Opt. Commun.*, Vol. 209, No. 4-6, Aug. 2002, pp. 427-436, ISSN 0030-4018

Liu, M. M. K. (1996). *Principles and Applications of Optical Communications.* Richard D. Irwin, ISBN 978-0256164152, Chicago

Lu, M. F.; Deng, J.-S.; Juang, C.; Jou, M. J. & Lee, B. J. (1995). Equivalent circuit model of quantum-well lasers. *IEEE J. Quantum Electron.*, Vol. 31, No. 8, Aug. 1995, pp. 1418-1422, ISSN 0018-9197

Mortazy, E. & Moravvej-Farshi, M. K. (2005). A new model for optical communication systems. *Opt. Fiber Technol.*, Vol. 11, No. 1, Jan. 2005, pp. 69-80, ISSN 1068-5200

Murakami, M.; Imai, T. & Aoyama, M. (1996). A remote supervisory system based on subcarrier overmodulation for submarine optical amplifier systems. *J. Lightwave Technol.*, Vol. 14, No. 5, May 1996, pp. 671-677, ISSN 0733-8724

Novak, S. & Gieske, R. (2002). Simulink model for EDFA dynamics applied to gain modulation. *J. Lightwave Technol.*, Vol. 20, No. 6, Jun. 2002, pp. 986-992, ISSN 0733-8724

Novak, S. & Moesle, A. (2002). Analytic model for gain modulation in EDFAs. *J. Lightwave Technol.*, Vol. 20, No. 6, Jun. 2002, pp. 975-985, ISSN 0733-8724

O'Mahony, M. J. (1988). Semiconductor laser optical amplifiers for use in future fiber systems. *J. Lightwave Technol.*, Vol. 6, No. 4, Apr. 1988, pp. 1556-1562, ISSN 0733-8724

Pederson, B.; Dybdal, K.; Hansen, C. D.; Bjarklev, A.; Povlsen, J. H.; Vendeltorp-Pommer, H. & Larsen, C. C. (1990). Detailed theoretical and experimental investigation of high-gain erbium-doped. *IEEE Photon. Technol. Lett.*, Vol. 2, No.12, Dec. 1990, pp. 863-865, ISSN 1041-1135

Rossi, G.; Paoletti, R. & Meliga, M. (1998). SPICE simulation for analysis and design of fast 1.55μm MQW laser diodes. *J. Lightwave Technol.*, Vol. 16, No. 8, Aug. 1998, pp. 1509-1516, ISSN 0733-8724

Settembre, M.; Matera, F.; Hagele, V.; Gabitov, I.; Mattheus, A. W. & Turitsyn, S. K. (1997). Cascaded optical communication systems with in-line semiconductor optical amplifiers. *J. Lightwave Technol.*, Vol. 15, No. 6, Jun. 1997, pp. 962-967, ISSN 0733-8724

Sharaiha, A. & Guegan, M. (2000). Equivalent circuit model for multi-electrode semiconductor optical amplifiers and analysis of inline photodetection in bidirectional transmissions. *J. Lightwave Technol.*, Vol. 18, No. 5, May 2000, pp. 700-707, ISSN 0733-8724

Shimizu, K.; Mizuochi, T. & Kitayama, T. (1993). Supervisory signal transmission experiments over 10000 km by modulated ASE of EDFAs. *Electron. Lett.*, Vol. 29, No. 12, Jun. 1993, pp. 1081-1083, ISSN 0013-5194

Simon, J. C. (1987). GaInAsP Semiconductor laser amplifier for single-mode optical fiber communications., *J. Lightwave Technol.*, Vol. 5, No. 9, Sep. 1987, pp. 1286-1295, ISSN 0733-8724

Sun, Y.; Luo, G.; Zyskind, J. L.; Saleh, A. A. M.; Srivastave, A. K. & Sulhoff, J. W. (1996). Model for gain dynamics in erbium-doped fibre amplifiers. *Electron. Lett.*, Vol. 32, No. 16, Aug. 1996, pp. 1490-1491, ISSN 0013-5194

Tsou, B. P. C. & Pulfrey, D. L. (1997). A versatile SPICE model for quantum-well lasers. *IEEE J. Quantum Electron.*, Vol. 33, No. 2, Feb. 1997, pp. 246-254, ISSN 0018-9197

Wu, A. W. T. & Lowery, A. J. (1998). Efficient multiwavelength dynamic model for erbium-doped fiber amplifier. *IEEE J. Quantum Electron.*, Vol. 34, No. 8, Aug. 1998, pp. 1325-1331, ISSN 0018-9197

Yu, Q. & Fan, C. (1999). Simple dynamic model of all-optical gain-clamped erbium-doped fiber amplifiers. *J. Lightwave Technol.*, Vol. 17, No. 7, Jul. 1999, pp. 1166-1171, ISSN 0733-8724

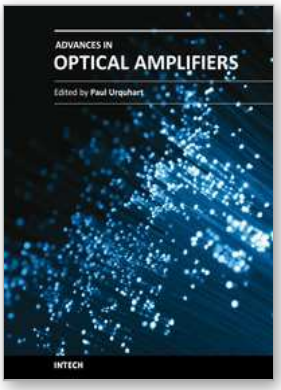

Advances in Optical Amplifiers

Edited by Prof. Paul Urquhart

ISBN 978-953-307-186-2
Hard cover, 436 pages
Publisher InTech
Published online 14, February, 2011
Published in print edition February, 2011

Optical amplifiers play a central role in all categories of fibre communications systems and networks. By compensating for the losses exerted by the transmission medium and the components through which the signals pass, they reduce the need for expensive and slow optical-electrical-optical conversion. The photonic gain media, which are normally based on glass- or semiconductor-based waveguides, can amplify many high speed wavelength division multiplexed channels simultaneously. Recent research has also concentrated on wavelength conversion, switching, demultiplexing in the time domain and other enhanced functions. Advances in Optical Amplifiers presents up to date results on amplifier performance, along with explanations of their relevance, from leading researchers in the field. Its chapters cover amplifiers based on rare earth doped fibres and waveguides, stimulated Raman scattering, nonlinear parametric processes and semiconductor media. Wavelength conversion and other enhanced signal processing functions are also considered in depth. This book is targeted at research, development and design engineers from teams in manufacturing industry, academia and telecommunications service operators.

How to reference

In order to correctly reference this scholarly work, feel free to copy and paste the following:

Jau-Ji Jou and Cheng-Kuang Liu (2011). Equivalent Circuit Models for Optical Amplifiers, Advances in Optical Amplifiers, Prof. Paul Urquhart (Ed.), ISBN: 978-953-307-186-2, InTech, Available from: http://www.intechopen.com/books/advances-in-optical-amplifiers/equivalent-circuit-models-for-optical-amplifiers

INTECH
open science | open minds

InTech Europe
University Campus STeP Ri
Slavka Krautzeka 83/A
51000 Rijeka, Croatia
Phone: +385 (51) 770 447
Fax: +385 (51) 686 166
www.intechopen.com

InTech China
Unit 405, Office Block, Hotel Equatorial Shanghai
No.65, Yan An Road (West), Shanghai, 200040, China
中国上海市延安西路65号上海国际贵都大饭店办公楼405单元
Phone: +86-21-62489820
Fax: +86-21-62489821